

Performance Trials of an Integrated Loran/GPS/IMU Navigation System, Part II

Gregory Johnson, Ruslan Shalaev, Christian Oates, *John J. McMullen Associates*
Richard Hartnett, Hunter Atherton, Michael Teixeira, *U.S. Coast Guard Academy*
Peter Swaszek, *University of Rhode Island*

BIOGRAPHY

Gregory Johnson is a Senior Program Manager at Alion Science & Technology, JJMA Maritime Sector. He heads up the New London, CT office which provides research and engineering support to the Coast Guard Academy and R&D Center. Recently he has been working on projects in Loran, DGPS and WAAS. He has over 16 years of experience in electrical engineering and R&D. Dr. Johnson holds a BSEE from the Coast Guard Academy (1987), a MSEE from Northeastern University (1993), and a Ph.D. in Electrical Engineering from the University of Rhode Island (2005).

Peter F. Swaszek is a Professor of Electrical and Computer Engineering at the University of Rhode Island. He received his Ph.D. in Electrical Engineering from Princeton University. His research interests are in digital signal processing with a focus on digital communications and navigation systems.

Richard J. Hartnett received the BSEE degree from the U. S. Coast Guard Academy (USCGA) in 1977, the MSEE degree from Purdue in 1980, and the Ph.D. EE from the University of Rhode Island in 1992. He holds the grade of Captain in the U. S. Coast Guard, and is Head of Electrical and Computer Engineering at the USCG Academy. CAPT Hartnett has been a faculty member at USCGA since 1985, and is serving as National Marine Representative, Institute of Navigation (ION) Council. He is the 2004 winner of the International Loran Association Medal of Merit.

ABSTRACT

The 2001 Volpe National Transportation Systems Center report on GPS vulnerabilities identified Loran-C as one possible backup system for GPS. The Federal Aviation Administration (FAA) observed in its recently completed Navigation and Landing Transition Study that Loran-C, as an independent radio navigation system, is theoretically the best backup for GPS; however, this study also observed that Loran-C's potential benefits hinge upon the level of position accuracy actually realized (as measured by the 2 drms error radius). For aviation applications this is the ability to support non-precision approach (NPA) at a Required Navigation Performance (RNP) of 0.3 which

equates to a 2 drms error of 309 meters and for marine applications this is the ability to support Harbor Entrance and Approach (HEA) with 8-20 m of accuracy. The recently released report of the DOT Radionavigation Task Force recommended to "complete the evaluation of enhanced Loran to validate the expectation that it will provide the performance to support aviation NPA and maritime HEA operations." To meet this need, the FAA is currently leading a team consisting of members from industry, government, and academia to provide guidance to the policy makers in their evaluation of the future of enhanced Loran (eLoran) in the United States. Through FAA sponsoring, the U.S. Coast Guard Academy (USCGA) is responsible for conducting some of the tests and evaluations to help determine whether eLoran can provide the accuracy, availability, integrity, and continuity to meet these requirements.

The key to meeting HEA accuracy requirements is an accurate ASF spatial grid. This can be met by a very dense grid of ASF values; however, this increases the problems with grid distribution and storage on the receiver. Previous work (ION AM June 2004) suggested that a sparse grid can be used and accuracy targets still reached by interpolating the points in between the grid values. The difficulty is in creating a grid with accurate grid point data. Several options for uniform grids were tested (ION NTM Jan 2005) and did not yield sufficient accuracy. In this work we have created a more accurate grid using non-uniform spacing and better matching of data to grid points. An integrated Loran/GPS/IMU receiver has been developed that incorporated this new ASF grid. This receiver integrates IMU information (velocity and acceleration) and ASF data from a stored grid into the Loran position solution to improve the accuracy and consistency of the resulting position. Initial results of this receiver were reported in (ION NTM Jan 2005). Since then, extensive work has been done to characterize the IMU errors and biases in order to better incorporate the IMU data into the integrated receiver. A Kalman filter is used to integrate the information and to predict forward the position to remove the time lag caused by the Loran filtering. The GPS information (position, time) is used to measure the ASF values in real-time to track deviations from the stored ASF grid. These grid differences are used to correct the grid values in the

absence of a local ASF monitor station. Performance of the receiver is presented using an ASF grid alone, an ASF grid corrected using temporal ASF variations from a local ASF monitor site, and an ASF grid corrected using the real-time calculated grid differences. Finally, how all of these efforts lead towards meeting the accuracy requirements is shown.

INTRODUCTION

Contrary to what some may believe, Loran-C is still alive and in use worldwide. The United States is served by the North American Loran-C system made up of 29 stations organized into 10 chains (see Figure 1). Loran coverage is available worldwide as seen in Figure 2.

Given the ubiquity and quality of service available from the Global Positioning Service (GPS), one might wonder of what use is a system that has been operational since the 1970's? The answer is that Loran is an excellent backup system for GPS. As discussed in many sources, such as the Volpe vulnerability study [1], GPS is vulnerable to both intentional and unintentional jamming. Since Loran is a totally different system and subject to different failure modes than GPS, it can act as an independent backup system that functions when GPS does not. The Federal Aviation Administration (FAA) observed in its recently completed Navigation and Landing Transition Study [2] that Loran-C, as an independent radio navigation system,

is theoretically the best backup for GPS; however, this study also observed that Loran-C's potential benefits hinge upon the level of position accuracy actually realized (as measured by the 2 drms error radius). For aviation applications this is the ability to support non-precision approach (NPA) at a Required Navigation Performance (RNP) of 0.3 which equates to a 2 drms error of 307 meters and for marine applications this is the ability to support Harbor Entrance and Approach (HEA) with 8-20 m of accuracy.

The goals to enable Loran to meet these requirements consist of two main parts. First is to develop an ASF correction approach. Methods need to be developed to account for ASFs to improve the accuracy of the Loran position in aviation and marine environments. Second is to develop an integrated receiver. This integrated receiver will use additional sensors to improve Loran position performance, reliability, and integrity.

This paper is a continuation of work presented in January [3]. In this paper we will first provide a background and description of ASF variations and the solution approaches for compensating for ASFs. We will then discuss the work on developing an accurate ASF grid and then the integrated receiver consisting of a Loran, GPS and IMU integrated using a Kalman filter as well as performance results.

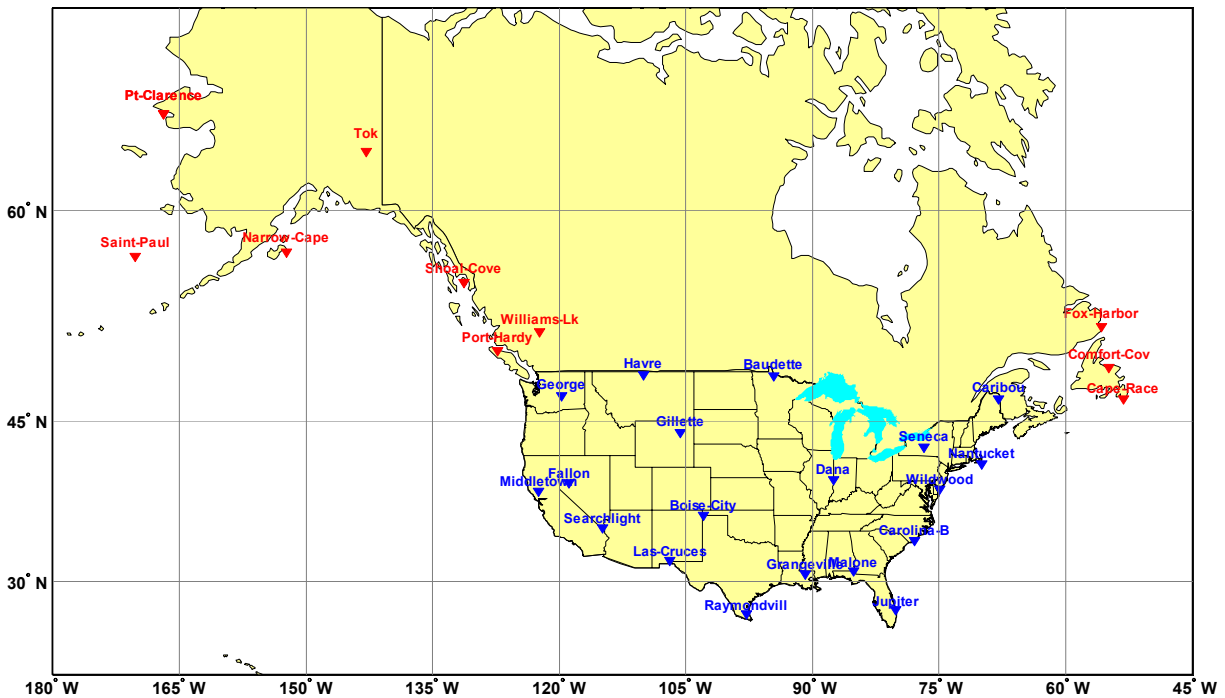


Figure 1 – North American Loran-C System.



Figure 2 – Worldwide Loran Coverage.

ASF SUMMARY

The biggest limitation on meeting the accuracy requirements is the spatial and temporal variations in Time of Arrival (TOA) observed by the receiver and presented to the position solution algorithm. This variation has been studied and presented in previous works [4-6]. The key to overcoming this limitation is having a good solution for Additional Secondary Factors (ASFs). A typical Loran receiver works on the simplifying assumption that the Loran signal propagates at a constant velocity – that of an electromagnetic wave in atmosphere over seawater. This is clearly not the case in most circumstances as the path from a given Loran station and a receiver may traverse a variety of terrain. The ASF accounts for the delay in the signal due to the propagation over non-seawater paths. This delay is due to terrain features; topography and obstacles along the path as well as the non-uniform (and lower) conductivity of land as opposed to seawater. The ASF value is used to adjust the receiver’s estimate of the TOA of the Loran signal. It can be in the range of 1 to 8 microseconds across the continental U.S. (CONUS). What is more troubling to a receiver is that it can vary by as much as 1 to 2 microseconds in a local area such as a harbor or airport. Since 10ns is equal to 3m, to meet the 20m requirement requires limiting the total system variation (including noise and other system deficiencies) to less than 65ns.

TEMPORAL ASF VARIATION

The temporal variation in the ASF is the variation over time seen in the measured TOA by a receiver in a static location. These variations are due to several effects:

diurnal (small, <100ns), seasonal (larger, slowly varying, >1000ns), weather related, and system time “errors” (20ns jumps, plus up to 1000ns offsets). Over short time periods the temporal change is negligible, over long periods it is not.

SPATIAL ASF VARIATION

The spatial variation in the ASF is the change in ASF value over an area due to differences in terrain (topography and conductivity). These spatial variations have been measured and evaluated extensively over the past several years (flight tests in August 2002, maritime tests in December 2002, flight and ground tests in Jul-Sep 2003, and local maritime tests from 2002-2005) and show that ASF variations can exceed 1 microsecond over a fairly small area (8km) – see Figure 3.

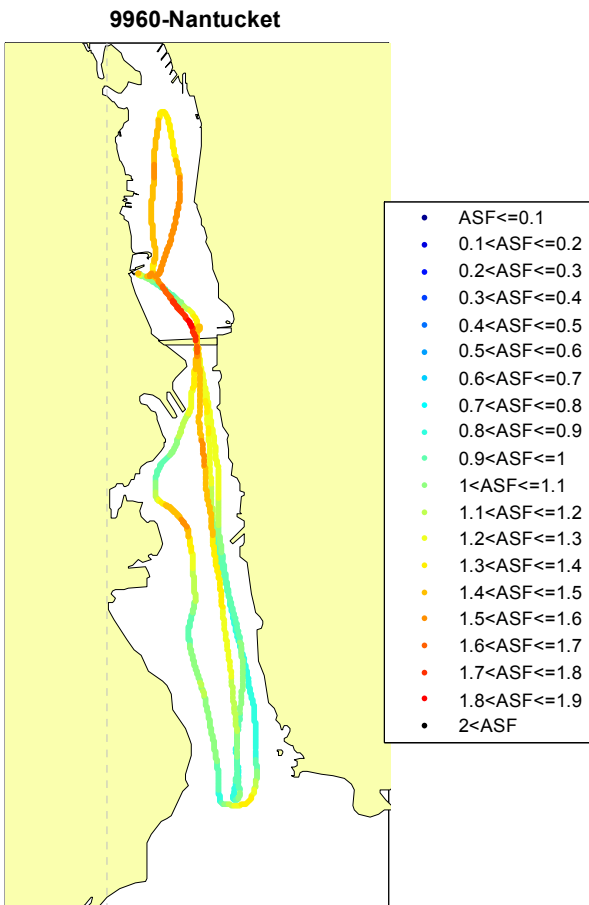


Figure 3 -- Nantucket ASF variations seen in the Thames River, CT.

In addition to these broader spatial variations, there are more localized effects due to large, metallic structures such as bridges. This variation is shown in Figure 4 for the position track shown in Figure 5.

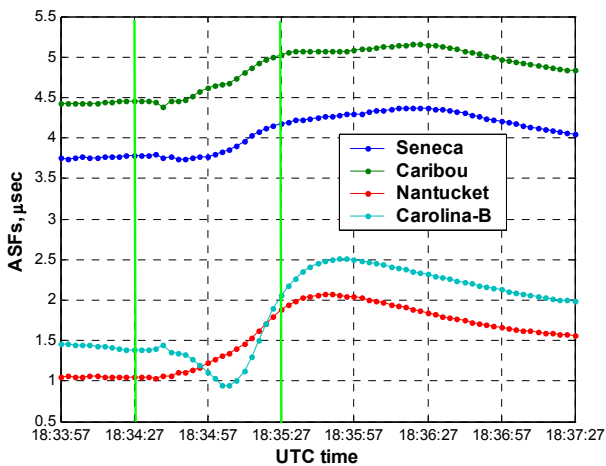
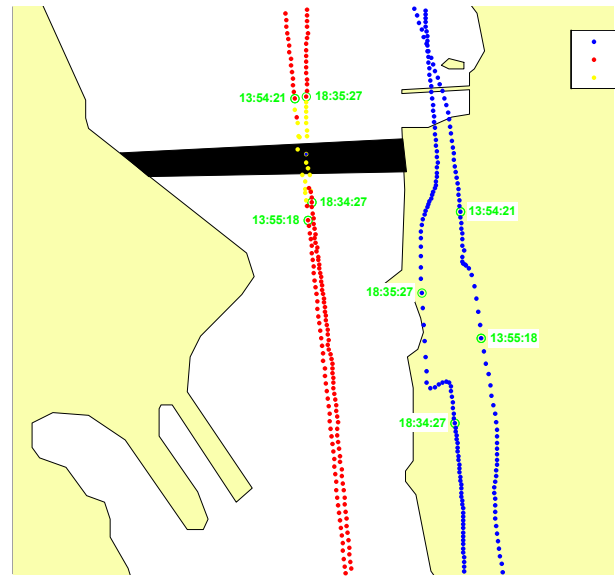


Figure 4 -- ASF variation due to passing under a large bridge.



Bearing from bridge to: Seneca=292; Caribou=27; Nantucket=93; Carolina-B=214;

Figure 5 – Position track showing times that vessel is under a bridge.

Another spatial effect is the change in ASF vs. altitude. This has been examined somewhat over the past two years (testing in Jan, May, and Sep 2003 and Oct 2004). There have been no conclusive results to date although the data does seem to indicate that there is an effect. Variations versus altitude are shown in Figure 6 for flights conducted along the same ground track near Atlantic City, NJ.

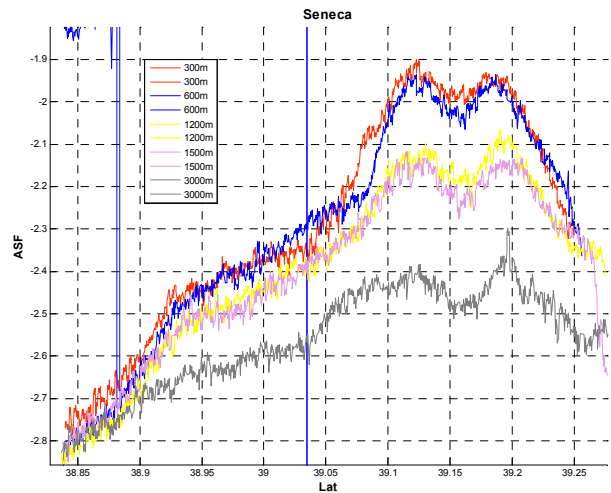


Figure 6 – Seneca ASF plotted vs. longitude for various altitudes. All altitudes flown along the same ground track in the same direction.

The final effect to be considered is the directional effect. This is discussed to great extent in our companion paper [7]. In short; however, the problem is that with most H-field (loop) antennas the measured TOA varies as the antenna is rotated. This is shown in Figure 7 where the

normalized ASFs for three Loran stations are plotted versus heading.

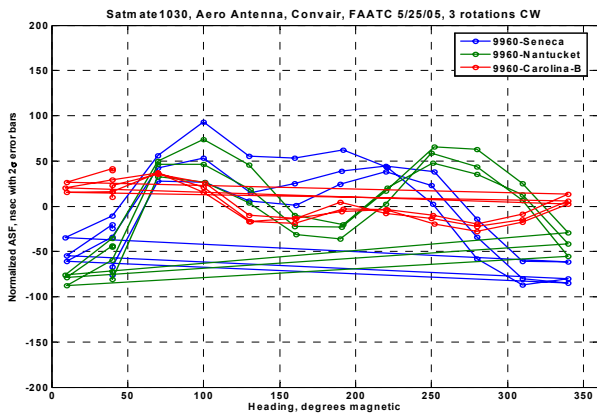


Figure 7 – Normalized ASFs for three Loran stations plotted vs. antenna heading.

In order to account for these variations and increase the position accuracy, the current strategy for Harbor Entrance and Approach (HEA) is as follows. A spatial grid of ASF values is used to capture the range of ASF values spatially and the receiver interpolates within this grid. Differential Loran corrections are used to provide temporal corrections to the spatial grid. One method for this is to use a local reference station and broadcast corrections. The other method is to have the user receiver generate the temporal grid corrections using an integrated GPS receiver.

ASF GRIDS

To date there has been much thought and work into developing methods to create ASF grids for a harbor area. Our initial thought on grids was to use a grid of left, right, and center channel points [8]. However, this idea was dropped as difficult to implement for complex channels. Research then focused on using a sparse rectangular grid. Using a sparser grid makes the distribution and storage of the ASF grids easier. Our research [9] suggested that a coarse grid of 7x12 points could be used and still retain sufficient accuracy. The receiver would interpolate between the grid points using bilinear interpolation. In addition a bootstrapping method for starting out with the grid was devised and tested for convergence [10].

There were however, some problems with using a uniform grid as discussed in [3]. The data collection suffers from several problems: many of the grid points are on land and thus not measurable by boat, there are several points for which no data was collected, and most troublesome, the data was not collected uniformly at/around each grid point. These issues are shown in Figure 8. The black points are collected somewhat uniformly around the grid point; however the green points are not. The median value for the green points is mapped

to a grid point some distance away and not the center of the measured data, introducing an error into the grid, especially significant for areas with sharp change in ASF.

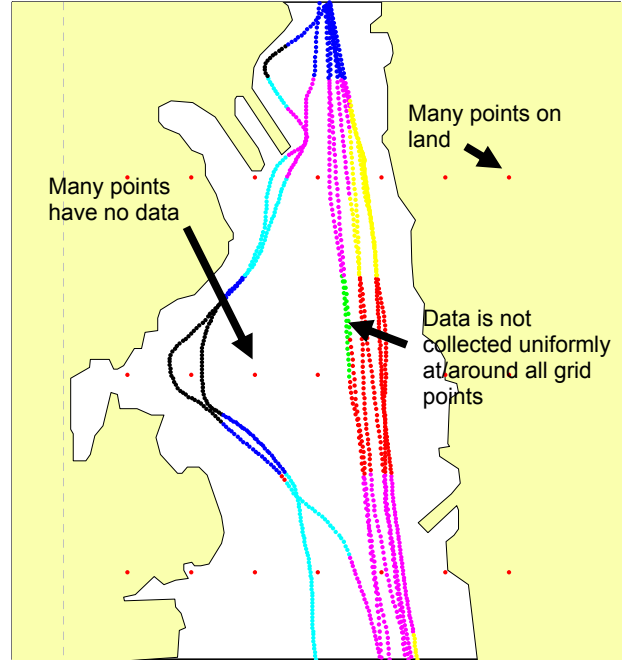


Figure 8 – Some of the problems with the uniform grid.

The results of applying the ASF grids to Loran TOAs are shown in Figure 9. In this figure, the green crosses are the GPS positions which are used as ground truth. The magenta points are the raw Loran positions which exhibit the typical 600m error offset from truth. The dark blue points are the positions calculated using the Loran data corrected using the BALOR grid ASFs interpolated using bilinear interpolation. The light blue points are a similar grid interpolation using the real ASF grid where grid points with no data were filled with an average value. The black points are the same real data with the grid points without data eliminated; with a triangular interpolation of the three closest grid points used. None of these grids gives great results due to the inaccuracies in the grids. If the actual ASF values were used the Loran+ASF track would be on top of the GPS track.

In the future we will investigate using non-uniform grids. Some possibilities include using K-means clustering to clump data to a grid point at the center of the cluster versus having the grid point locations determined a priori based on an even rectangular grid. Other options are to grid only those areas of interest such as channels and navigable areas versus a rectangle over the entire area. This leads to vectors of Lat, Long and ASFs versus an even grid. There are interpolation techniques such as a triangular interpolation (surface fit) that can be used though. A 1 ns quantization on the ASF data is probably sufficient; however, sufficient data needs to be taken at

each grid point such that the measurement noise is low (low standard deviation).

A typical procedure might then be as follows:

- Perform ASF predictions for the area using BALOR.
- Conduct a quick survey to verify the predictions.
- Select points for measurement based upon the predictions for the area and simulation of required density.
- Make accurate measurements at the selected points.

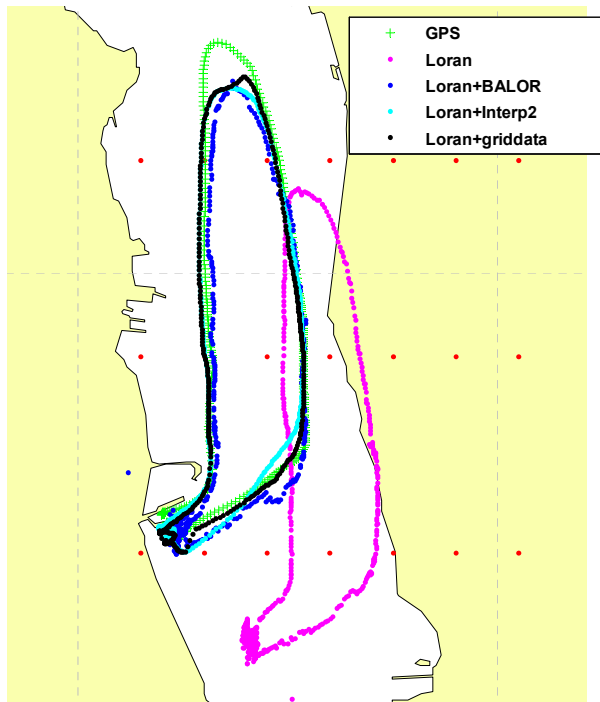


Figure 9 – ASF grid performance.

INTEGRATED RECEIVERS (HISTORICAL)

Loran was originally implemented by the Coast Guard in the 1970's as a maritime radionavigation system. The FAA adopted it as an aviation radionavigation system in the 1980's and certified it for en-route navigation. In the late 1980's the GPS system was being implemented with an IOC (initial operating capability) planned for 1991 and the FAA began investigating the use of GPS for in-flight navigation. The concern at that time was that the initial GPS system of 21 satellites with a planned IOC of 1991 would not meet the availability and integrity requirements for a sole means navigation system. Single satellite outages were predicted to cause loss of availability with a constellation of 21 satellites. GPS can use RAIM (receiver autonomous integrity monitoring) to provide fault detection – but it is not capable of adequate fault isolation alone (it needs some other navigation system

integrated with it). This spurred a number of people to investigate the use of integrated GPS and Loran receivers.

The focus of integrated GPS/Loran receivers in the 1980's and 1990's was to improve performance in the presence of Selective Availability, improve availability, improve integrity, and help in urban canyon environments. However, most of these drivers for an integrated receiver no longer exist: SA is turned off, the current GPS system has 24+ satellites providing much better availability, and WAAS provides integrity. Current research into integrated GPS/Loran receivers is now focused on improving Loran performance and providing a backup system in case of GPS outages.

INTEGRATED LORAN-IMU-(GPS) RECEIVER

The motivation for using an integrated receiver is that an accurate position source is needed in the absence of GPS. The ASFs correct for the major source of error in a Loran position; however, 20m is a difficult accuracy target to attain. It is important to account for Loran receiver errors as well to meet the 20m target.

The concept for an integrated Loran/GPS/IMU receiver is as follows. The Loran receiver measures the TOAs and applies the ASF correction using a stored ASF spatial grid as discussed above. The IMU provides heading and velocity information that is integrated with the Loran TOA measurements in order to smooth out the TOA measurements and prevent position jumps due to receiver errors. The Loran TOAs are not integrated with the GPS pseudoranges as the Loran receiver really does nothing to improve the GPS position solution. The intent is to have a receiver that can continue to provide accurate positions (Loran/IMU only) in the absence of GPS and function independently of GPS. The GPS receiver is used to track the ASF values in real-time in order to calculate the temporal correction to the ASF spatial grid. This temporal correction is updated as long as GPS is present. If and when GPS is lost, this temporal correction is then used to correct the spatial grid when the spatial grid is used in the Loran position solution. This part of the process could be replaced by using temporal updates in an area with differential Loran.

INERTIAL MEASURING UNIT (IMU)

The IMU we have chosen to use is a MEMs-based unit from Crossbow, Inc. (Figure 10). This unit, like other units based on MEMs technology, is low-cost but has poor long-term stability. This unit provides linear accelerations as well as angular velocities as shown in Figure 11. The IMU is typically mounted such that the x-axis is towards the front of the vessel, the y-axis is to the right, and the z-axis is thus down (see Figure 12). The IMU provides linear accelerations (a_x, a_y, a_z) along these axes. The IMU also provides the angular velocities

$(\omega_\phi, \omega_\theta, \omega_\psi)$ of the rotations around these axes (ϕ, θ, ψ) where ϕ is the rotation around the x-axis called the roll, θ is the rotation about the y-axis called the pitch, and ψ is the rotation about the z-axis called yaw. In all cases, the direction of positive rotation can be found using the right-hand rule.



Figure 10 – Crossbow IMU

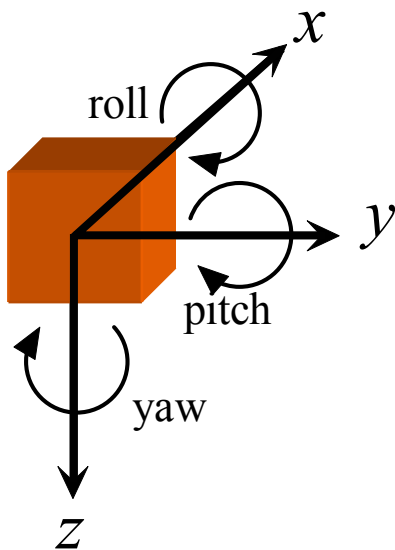


Figure 11 – IMU axis orientation.



Figure 12 – IMU axis orientation on a vessel.

The typical performance of this unit is shown in Figure 13 and Figure 14 which show data collected on the Thames River. The blue lines are the raw acceleration data that have been un-biased. The red lines are the filtered data. Due to the noise present in the data, filtering is necessary.

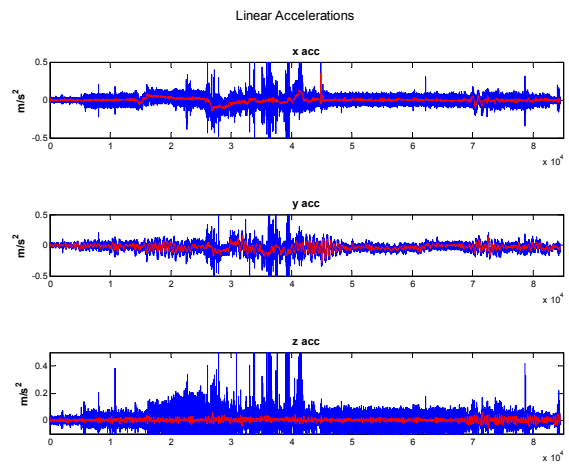


Figure 13 – IMU Linear acceleration data.

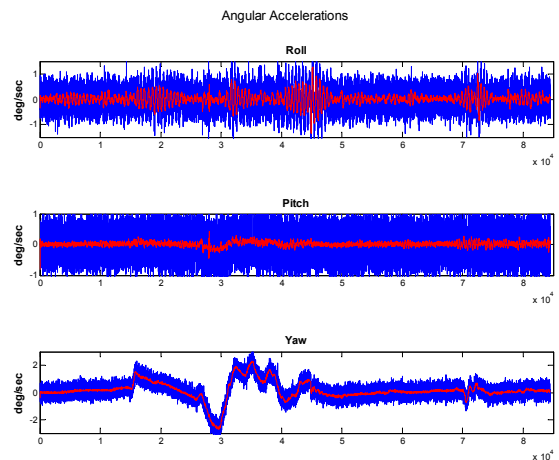


Figure 14 – Angular acceleration data.

These measurements can be integrated to provide velocities and changes in unit attitude. One issue with an IMU is that all of the measurement data (linear accelerations and angular velocities) are relative to the coordinate frame of the IMU. Thus, the linear acceleration in the IMU body frame must be converted into the respective accelerations in the navigation frame of East, North, Up (see Figure 15). This is a two-step process; first the attitude of the IMU must be tracked (by integrating the angular accelerations and adding to the current roll, pitch, and yaw angles). Then this attitude relative to the body frame is used to construct a rotation matrix to rotate the (x,y,z) accelerations into the accelerations relative to (E,N,U) . This is a fairly standard procedure and is discussed in [11, 12]. In order to ensure the rotation

matrices matched the East-North-Up navigation axis definition being used, the work was redone independently. The rotation matrices thus derived to convert between the IMU body frame and the navigation frame are as follows:

Rotation about x-axis:

$$R_x(\phi) = \begin{bmatrix} 0 & \cos \phi & \sin \phi \\ 1 & 0 & 0 \\ 0 & \sin \phi & -\cos \phi \end{bmatrix}$$

Rotation about the y-axis:

$$R_y(\theta) = \begin{bmatrix} 0 & 1 & 0 \\ \cos \theta & 0 & -\sin \theta \\ -\sin \theta & 0 & -\cos \theta \end{bmatrix}$$

Rotation about the z-axis:

$$R_z(\psi) = \begin{bmatrix} \sin \psi & \cos \psi & 0 \\ \cos \psi & -\sin \psi & 0 \\ 0 & 0 & -1 \end{bmatrix}$$

where at 0 degrees roll, pitch, and yaw, the x and N axes are aligned, the y and E axes are aligned, and the z and U axes are in opposite directions. The combined rotation matrix from body frame coordinates into navigation frame coordinates is: $R_z R_y R_x$.

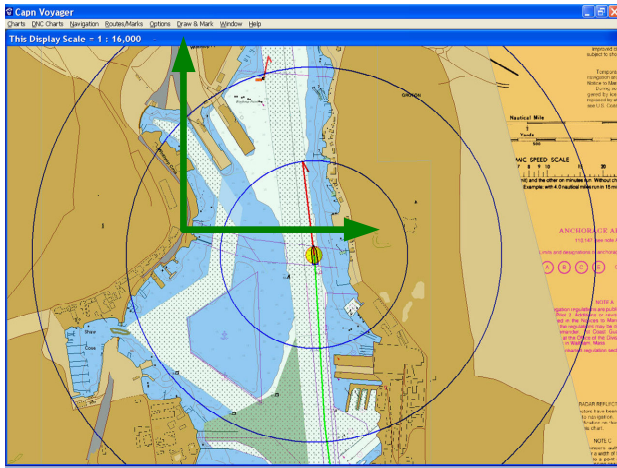


Figure 15 –Navigation Frame axes: East, North, Up.

IMU PROCEDURE

Currently the Loran-IMU integration is not done in real-time. The IMU data (raw data, 2 bytes for each of the 6 measurements) is collected at approximately 130 Hz and

saved to a file time-tagged by a GPS receiver to the nearest 0.1 seconds (so there are up to 14 data points with the same GPS time-tag). In post-processing the first step is to filter this data down to 1 second updates. The data is converted from the raw byte format into the accelerations in m/sec^2 and angular velocities in $rads/sec$ (combine bytes, convert from 2's complement to signed integer, scale, remove bias). The data points for each 1 second interval are averaged, which is the equivalent of a doing a lowpass filtering with a $\sim 130^{th}$ order FIR filter. This filtered data, accelerations (a_x, a_y, a_z) and angular velocities $(\omega_\phi, \omega_\theta, \omega_\psi)$ at 1 second intervals, is saved to a new file. The linear accelerations can then be integrated into velocities and the angular velocities integrated into attitude changes.

KALMAN FILTER

To integrate the IMU with the Loran data we have implemented an extended Kalman filter. In the extended Kalman filter, the IMU is used to create the reference trajectory. The IMU data is used to predict forward to the next position. This predicted position is used to calculate the TOAs and is also used to interpolate in the ASF grid to get the ASF values. The differences between these predicted TOAs and the measured TOAs (corrected by the ASF value) are taken. The differences are checked for possible cycle slips, and corrected if necessary, and then these TOA errors (differences between predicted and measured) are used as the input to the Kalman filter. The output of the Kalman filter is the position error which is used to correct the predicted position.

IMU ERROR MODEL FOR KALMAN FILTER

A model of the errors in the IMU is used from Brown [13]. However, since the extended Kalman filter will operate on the errors in the position domain, this model needs to be in the navigation frame, so the model is rewritten to be consistent with the navigation frame notation.

North channel:

$$\begin{aligned} \Delta \ddot{n} &= a_n + g \phi_e \\ -\dot{\phi}_e &= \frac{1}{R_{earth}} \Delta \dot{n} + \omega_n \phi_u - \epsilon_e \end{aligned}$$

East channel:

$$\begin{aligned} \Delta \ddot{e} &= a_e - g \phi_n \\ \dot{\phi}_n &= \frac{1}{R_{earth}} \Delta \dot{e} + \omega_e \phi_u + \epsilon_n \end{aligned}$$

Up channel:

$$\Delta \ddot{u} = a_u$$

Platform azimuth:

$$\dot{\phi}_u = \varepsilon_u$$

where (replacing x with e, n, or u):

- Δx = position error
- $\Delta \dot{x}$ = velocity error
- $\Delta \ddot{x}$ = acceleration error
- ϕ_x = platform error relative to level
- g = gravitational acceleration
- R_{earth} = earth radius
- a_x = accelerometer noise
- ε_x = gyro noise

This leads to a 9-state dynamic model $\Delta \mathbf{x}$:

1. east position error (m) -- Δe
2. east velocity error (m/sec) -- $\Delta \dot{e}$
3. platform tilt about North axis (rad) -- ϕ_n
4. north position error (m) -- Δn
5. north velocity error (m/sec) -- $\Delta \dot{n}$
6. platform tilt about -East axis (rad) -- $-\phi_e$
7. up position error (m) -- Δu
8. up velocity error (m/sec) -- $\Delta \dot{u}$
9. platform azimuth error (rad) -- ϕ_u

A Kalman Filter is built for the random process to be estimated that has the form:

$$\mathbf{x}_{k+1} = \Phi_k \mathbf{x}_k + \mathbf{w}_k$$

with the accompanying observation (measurement) equation:

$$\mathbf{z}_k = \mathbf{H}_k \mathbf{x}_k + \mathbf{v}_k$$

Classical Kalman filtering begins with an estimate of the state $\hat{\mathbf{x}}_0^-$ and its covariance matrix \mathbf{P}_0^- . Given N observations, the actual filtering is the iteration over k , $k = 1, 2, \dots, N$, of four steps: (illustrated in Figure 16)

- Project the state vector and its covariance matrix ahead one time step.
- Compute the Kalman filter gain.
- Update the estimate with the observations.
- Compute the error covariance for the updated estimate.

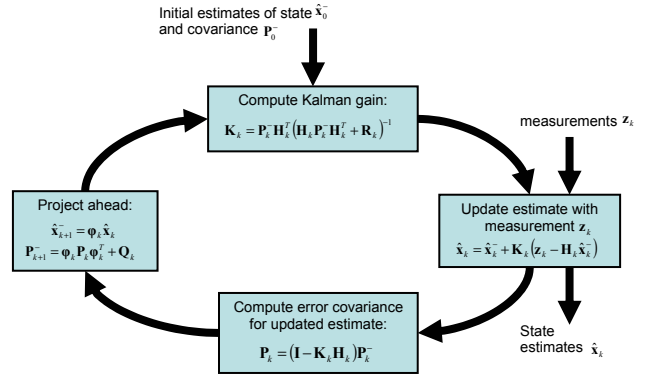


Figure 16 – Standard Kalman filter loop.

IMU RESULTS

Figure 17 shows the results of one trial in the position domain. The GPS track (ground truth) is shown in green. The raw Loran is shown in red (typical ~600m offset to the Southeast). The blue track is the Loran corrected using best-case ASF values (ASF values interpolated from the grid based upon the GPS position). The blue dots on top of the red are instances where the interpolation routine failed to return a valid value and 0 was used (no ASF is the same as raw Loran). The black track is the integrated Loran/IMU. The position error between each IMU position and the corresponding GPS position is shown in Figure 18.

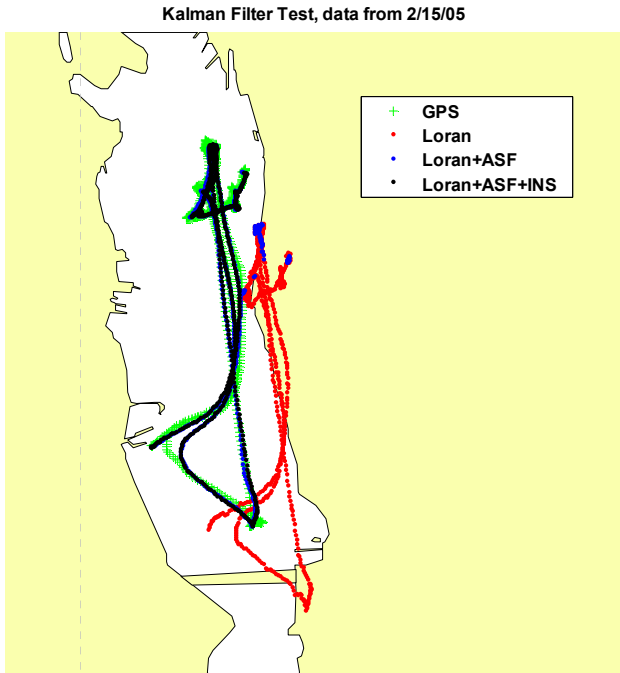


Figure 17 – Integrated Receiver test results, position domain.

The Loran solution performance is very sensitive to the accuracy of the ASF grid. At each position, the ASF grid error is calculated by subtracting the ASF value interpolated from the grid from the true ASF value (as measured during the data collection). This gives an idea of how well the grid is performing (plotted for the previous trial in Figure 18). Based on the results to date, further work is needed on grid development for the maritime application as previously discussed.

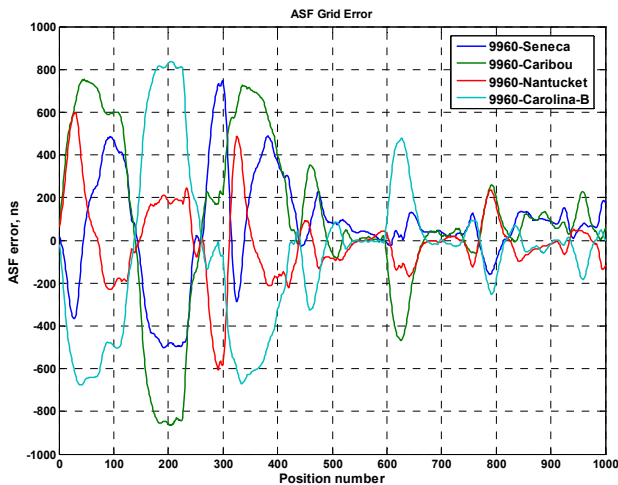


Figure 18. ASF grid error vs. time step during integrated receiver trial.

In order to test the filter performance various errors were introduced. First, cycle slips on Seneca (master) were introduced from time steps 60 to 65. This is shown in

Figure 20 by the magenta dots; no effect on the position solution is seen showing that the cycle slip detection and correction algorithm is working. Next, Loran errors were introduced at time steps 75-85 by reducing the SNR values by 60 dB, resulting in effectively no Loran signal. This is seen in Figure 19 by the cyan dots. Here, the impact of the unaided IMU is seen; the position starts to drift over time (remember each dot is 5 seconds apart). The third error introduced was to simulate the loss of the IMU information for time steps 160-190 by setting all IMU measurements (accelerations and angular velocities) to zero. This is effectively a linearized Kalman filter as there is no updating of the reference profile. This had minimal impact on the position solution (yellow dots in Figure 19). The real strength of the Kalman filter integrated receiver can be seen in cases when partial information is available. In Figure 20 the cyan dots are where two out of the four Loran stations are lost (simulated as above). A typical Loran receiver cannot navigate with only 2 Loran stations; here the integrated receiver is able to navigate very well with only two Loran stations and the IMU data.

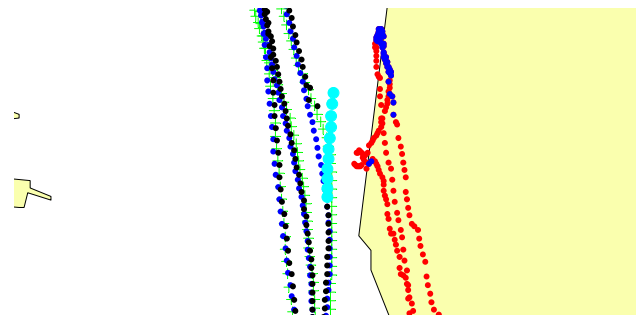


Figure 19 – Integrated receiver performance with loss of all Loran information.

Kalman Filter Test, data from 2/15/05

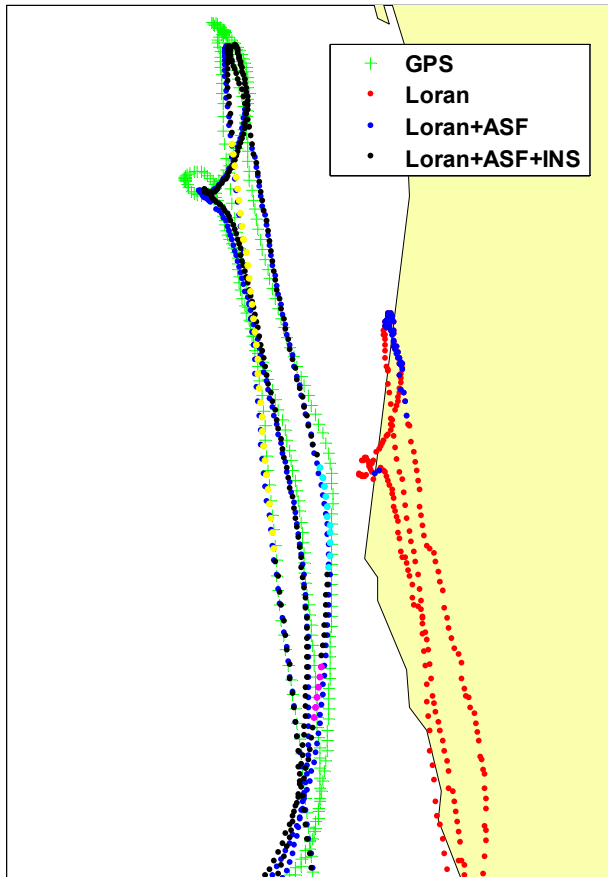


Figure 20 – Integrated receiver performance with injected errors.

CONCLUSIONS / FUTURE

Our integration approach for Loran based maritime navigation has been staged. First, a loosely coupled Loran/heading sensor (magnetic compass) system [14], next adding GPS system to estimate spatial and temporal ASFs [8], and then tightly coupling an IMU to the Loran data with ASF grids and ASF temporal corrections via GPS [3]. Continuing this latter work, we have in this paper more fully integrated our Loran/IMU/(GPS) system.

Such a system allows for easy transition from a primarily GPS-based solution to a high precision Loran solution during GPS outages. As demonstrated, the IMU can aid in Loran cycle slip detection. While we have not been exhaustive, it is clear that multiple integrated navigation solutions using data insufficient for a single approach are possible. Our example included 2 Loran signals and the IMU. Mixtures of GPS pseudoranges, Loran TOAs, and IMU could be considered. Future work will consider such integration.

The Loran solution performance is very sensitive to the accuracy of the ASF grid. Based on the results to date, further work is needed on grid development for the maritime application. We will focus in the future on using a non-uniform versus a uniform grid and measuring the ASFs on the grid accurately. Further work is also needed on the IMU. We need a better estimate of the IMU bias so it can be removed. We also need to integrate the IMU into the system in real-time vice in a post-process mode.

The Kalman filter appears to work to smooth the position solutions; however it needs to be fine-tuned. We also need to extend it into a predictor to account for the Loran position lag due to the filtering (averaging of pulses) in the Loran receiver.

ACKNOWLEDGMENTS

The authors would like to thank the Mr. Ken Dykstra of Alion-JJMA who provided assistance and Mr. Mitch Narins of the FAA who is the sponsor of this work.

REFERENCES

- [1] "Vulnerability Assessment of the Transportation Infrastructure Relying on the Global Positioning System," Volpe National Transportation Systems Center, U.S. Department of Transportation, Office of Ass't Sec for Transportation Policy, Boston, MA, August 2001.
- [2] "Navigation and Landing Transition Strategy," Federal Aviation Administration, Office of Architecture and Investment Analysis, ASD-1, Washington, DC, August 2002.
- [3] G. Johnson, R. Shalaev, P. Swaszek, and R. Hartnett, "Performance Trials of an Integrated Loran/GPS/IMU Navigation System, Part I," *proceedings of the Institute of Navigation, National Technical Meeting*, San Diego, CA, 24 - 27 January 2005.
- [4] R. Hartnett, G. Johnson, P. F. Swaszek, and M. J. Narins, "A Preliminary Study of LORAN-C Additional Secondary Factor (ASF) Variations," *proceedings of the 31st Annual Meeting, International Loran Association*, Washington, DC, 28-30 October 2002.
- [5] G. Johnson, R. Hartnett, P. Swaszek, K. Gross, C. Oates, and M. Narins, "FAA Loran-C Propagation Studies," *proceedings of the National Technical Meeting, Institute of Navigation*, Anaheim, CA, 22-24 January 2003.
- [6] G. Johnson, R. Hartnett, P. Swaszek, T. Moyer, and R. Shalaev, "Summer Vacation 2003 - ASF Spatial Mapping in CO, AR, FL, and CA," *proceedings of*

the 32nd Annual Meeting, International Loran Association, Boulder, CO, 3-6 November 2003.

- [7] G. Johnson, P. Swaszek, R. Hartnett, K. Dykstra, and R. Shalaev, "Airframe Effects on Loran H-field Antenna Performance," *proceedings of the Institute of Navigation Annual Meeting*, Cambridge, MA, 27 - 29 June 2005.
- [8] R. Hartnett, P. Swaszek, and G. Johnson, "Integrated GPS/Loran Receiver for ASF Propagation Studies," *proceedings of the ION-GPS 2003*, Portland, OR, 9-11 Sep 2003.
- [9] R. Hartnett, G. Johnson, and P. Swaszek, "Navigating Using an ASF Grid for Harbor Entrance and Approach," *proceedings of the Institute of Navigation, Annual Meeting*, Dayton, OH, 6 - 9 June 2004.
- [10] G. Johnson, R. Shalaev, R. Hartnett, and P. Swaszek, "Can Loran Meet GPS backup Requirements?" *proceedings of the 11th Saint Petersburg International Conference on Integrated Navigation Systems*, Saint Petersburg, RU, 24 - 26 May 2004.
- [11] J.-H. Wang, "The Aiding of a Low-Cost MEMS INS for Land Vehicle Navigation Using Fuzzy Logic Expert System," *proceedings of the Institute of Navigation, GNSS Conference*, Long Beach, CA, 21 - 24 September 2004.
- [12] K. J. Walchko, "Low Cost Inertial Navigation: Learning to Integrate Noise and Find Your Way," in *Graduate School*: University of Florida, 2002.
- [13] R. G. Brown and P. Y. Hwang, *Introduction to Random Signals and Applied Kalman Filtering*, 3rd ed. New York: John Wiley & Sons, 1997, pp.
- [14] P. Swaszek, G. Johnson, C. Oates, R. Hartnett, and G. Weeks, "A Demonstration of High Accuracy Loran-C for Harbor Entrance and Approach Areas," *proceedings of the Fifty-ninth Annual Meeting, Institute of Navigation*, Albuquerque, NM, 23-25 June 2003.

DISCLAIMER AND NOTE

The views expressed herein are those of the authors and are not to be construed as official or reflecting the views of the U.S. Coast Guard, Federal Aviation Administration, or any agency of the U.S. Government.